Peyer's patches (*26*). Seemingly unstable Foxp3 expression observed in these and other studies (*21*) can be due to cellular stress, the presence of few contaminating Foxp3$^-$ cells or cells which underwent transient Foxp3 up-regulation, or recently generated Foxp3$^+$ cells on their way to stable Foxp3 expression yet still able to expand and differentiate into effector T cells in lymphopenic or nonlymphopenic settings. Consistent with the latter notion, loss of Foxp3 expression by a minor population of YFP$^+$ cells was observed during induction of Foxp3 in peripheral YFP$^-$GFP$^-$CD4$^+$ T cells under lymphopenic conditions. In contrast, YFP$^+$GFP$^+$ $T_{reg}$ cells maintained Foxp3 expression in these experiments (fig. S13). Furthermore, transient expression of Foxp3 during retinoic acid receptor (RAR)–related orphan receptor–γ (RORγ)–dependent differentiation of Th17 cells was visualized through activation of the R26Y allele by Cre recombinase constitutively expressed under control of the endogenous *Foxp3* locus (*27*). Additionally, differences in regulation of expression of *Foxp3* bacterial artificial chromosome (BAC) transgene and the endogenous *Foxp3* locus encoding Cre can also affect the discrepant outcomes of YFP-tagging of $T_{reg}$ cells in the corresponding experimental models.

We demonstrated that the $T_{reg}$ cell lineage is remarkably stable under physiologic conditions and after a variety of challenges. Stable Foxp3 expression in committed $T_{reg}$ cells is probably facilitated by a positive autoregulatory loop (*28*). Our results also suggest that continuous self-renewal of the established $T_{reg}$ cell population combined with heritable maintenance of Foxp3 expression serves as a major mechanism of maintenance of this lineage in adult mice.

### References and Notes


1. F. el Marjou *et al.*, *Genesis* **39**, 186 (2004).
2. Y. Dor, J. Brown, O. I. Martinez, D. A. Melton, *Nature* **429**, 41 (2004).
3. J. D. Fontenot, M. A. Gavin, A. Y. Rudensky, *Nat. Immunol.* **4**, 330 (2003).
4. J. D. Fontenot *et al.*, *Immunity* **22**, 329 (2005).
5. S. Hori, T. Takahashi, S. Sakaguchi, *Adv. Immunol.* **81**, 331 (2003).
6. R. Khattri, T. Cox, S.-A. Yasayko, F. Ramsdell, *Nat. Immunol.* **4**, 337 (2003).
7. J. M. Kim, J. P. Rasmussen, A. Y. Rudensky, *Nat. Immunol.* **8**, 191 (2007).
8. I. Apostolou, A. Sarukhan, L. Klein, H. von Boehmer, *Nat. Immunol.* **3**, 756 (2002).
9. C.-S. Hsieh *et al.*, *Immunity* **21**, 267 (2004).
10. M. S. Jordan *et al.*, *Nat. Immunol.* **2**, 301 (2001).
11. R. Pacholczyk, H. Ignatowicz, P. Kraj, L. Ignatowicz, *Immunity* **25**, 249 (2006).
12. L. M. Williams, A. Y. Rudensky, *Nat. Immunol.* **8**, 277 (2007).
13. Materials and methods are available as supporting material on *Science* Online.
14. W. Liao *et al.*, *Nat. Immunol.* **9**, 1288 (2008).
15. M. A. Burchill, J. Yang, C. Vogtenhuber, B. R. Blazar, M. A. Farrar, *J. Immunol.* **178**, 280 (2007).
16. R. Setoguchi, S. Hori, T. Takahashi, S. Sakaguchi, *J. Exp. Med.* **201**, 723 (2005).
17. J. D. Fontenot, J. P. Rasmussen, M. A. Gavin, A. Y. Rudensky, *Nat. Immunol.* **6**, 1142 (2005).
18. A. L. Bayer, A. Yu, T. R. Malek, *J. Immunol.* **178**, 4062 (2007).
19. T. R. Malek *et al.*, *J. Clin. Immunol.* **28**, 635 (2008).
20. G. Oldenhove *et al.*, *Immunity* **31**, 772 (2009).
21. X. Zhou, S. Bailey-Bucktrout, L. T. Jeker, J. A. Bluestone, *Curr. Opin. Immunol.* **21**, 281 (2009).
22. M. A. Koch *et al.*, *Nat. Immunol.* **10**, 595 (2009).
23. J. D. Katz, B. Wang, K. Haskins, C. Benoist, D. Mathis, *Cell* **74**, 1089 (1993).
24. H. J. Wu *et al.*, *Immunity* **32**, 815 (2010).
25. X. Zhou *et al.*, *Nat. Immunol.* **10**, 1000 (2009).
26. M. Tsuji *et al.*, *Science* **323**, 1488 (2009).
27. L. Zhou *et al.*, *Nature* **453**, 236 (2008).
28. Y. Zheng *et al.*, *Nature* **463**, 808 (2010).


29. We thank K. Forbush, T. Chu, L. Karpik, A. Bravo, J. Herlihy, P. Zarin, G. Gerard, A. Ortiz-Lopes, and K. Hattori for assistance with mouse colony management; F. Costantini for R26Y mice; V. Kuchroo for Foxp3-IRES-GFP mice; P. Chambon for Cre-ERT2 plasmid; E. Pamer, C. Shi, and E. Leiner for *L. monocytogenes* and assistance with experiments; and P. Fink and K. Simmons for cells from Rag2pGFP mice and helpful discussion. R.E.N. was supported by NIH Medical Scientist Training Program grant GM07739. A.Y.R. is an investigator with the Howard Hughes Medical Institute, and this work was also supported by grant AI51530 from the NIH to C.B. and D.M.


### Supporting Online Material

www.sciencemag.org/cgi/content/full/329/5999/1667/DC1
Materials and Methods
Figs. S1 to S13

7 May 2010; accepted 2 August 2010
10.1126/science.1191996



# Dendritic Discrimination of Temporal Input Sequences in Cortical Neurons

**Tiago Branco, Beverley A. Clark, Michael Häusser***

**The detection and discrimination of temporal sequences is fundamental to brain function and underlies perception, cognition, and motor output. By applying patterned, two-photon glutamate uncaging, we found that single dendrites of cortical pyramidal neurons exhibit sensitivity to the sequence of synaptic activation. This sensitivity is encoded by both local dendritic calcium signals and somatic depolarization, leading to sequence-selective spike output. The mechanism involves dendritic impedance gradients and nonlinear synaptic *N*-methyl-D-aspartate receptor activation and is generalizable to dendrites in different neuronal types. This enables discrimination of patterns delivered to a single dendrite, as well as patterns distributed randomly across the dendritic tree. Pyramidal cell dendrites can thus act as processing compartments for the detection of synaptic sequences, thereby implementing a fundamental cortical computation.**

In sensory pathways, the relative timing of spikes from different neuronal populations can represent features of stimuli (*1*–*4*). A fundamental problem in cortical sensory processing is, thus, the discrimination of different spatiotemporal sequences of inputs (*5*). Although networks composed of simple neurons can, in principle, decode temporal sequences, the size and complexity of such networks can be greatly reduced if individual neurons can perform temporal decoding (*6*, *7*). Dendritic trees might contribute to this decoding, because they are highly nonlinear devices that can locally process and integrate synaptic signals (*8*–*10*). For example, spatiotemporally clustered inputs trigger dendritic spikes (*11*–*15*), which can generate independent functional subunits, enhancing the computational potential of the neuron (*16*–*18*) and encoding spatial and temporal input synchrony. Whether these nonlinear dendritic properties can be exploited to perform higher-order computations such as temporal sequence detection is unknown. In 1964, Wilfrid Rall predicted that, because dendrites act as a delay line, activation of synapses along a dendrite in different directions should produce different responses at the soma (*19*). Although the dendrites of retinal neurons exhibit such direction selectivity (*20*–*22*), experimental investigation of the sensitivity to spatiotemporal sequences of synaptic activation in cortical pyramidal cell dendrites has been a challenge due to the difficulty in delivering the spatiotemporal input patterns with the necessary submillisecond and submicron precision.

To test the sensitivity of single dendrites to the order of activation of a defined set of synapses, we controlled spatiotemporal input patterns using multisite, two-photon glutamate uncaging at identified dendritic spines (*15*, *23*) in layer 2/3 pyramidal neurons of somatosensory and visual cortex. We first studied the sensitivity of single dendrites to an ordered sequence of synaptic activation in opposite directions, selecting 8 to 10 spines on single basal and apical oblique dendritic branches (Fig. 1, A and B). Activating each site in isolation (Fig. 1C) produced synaptic responses [glutamate excitatory postsynaptic potentials (gluEPSPs)] within physiological parameters (fig. S1). Sequential activation of spines from the dendritic branch to the soma (IN) or from the soma to the tip (OUT) produced strongly directionally sensitive responses. The IN direction always produced a larger somatic response than the OUT direction (Fig. 1, D and E) (31 ± 4% increase, $P < 0.0001$,

Wolfson Institute for Biomedical Research and Department of Neuroscience, Physiology, and Pharmacology, University College London, Gower Street, London WC1E 6BT, UK.

*To whom correspondence should be addressed. E-mail: m.hausser@ucl.ac.uk

$n$ = 20 observations, corresponding to a mean peak voltage difference of 2.8 ± 0.4 mV), even when stimulating only three inputs (fig. S2). The EPSP peak was dependent on input velocity (Fig. 1, F and G), with optimal direction sensitivity at 2.6 ± 0.5 μm/ms (Fig. 1H). Axonal action potential output was highly directionally sensitive, with a higher spike probability in the IN direction than the OUT direction (38 ± 9% increase, $P$ = 0.0013, $n$ = 7) (Fig. 1, I to K).

The readout of sequence sensitivity was not just electrical but also chemical, as local dendritic $Ca^{++}$ signals also showed strong direction and velocity sensitivity (Fig. 2, A to C). Peak local dendritic $Ca^{++}$ signals were always larger in the IN versus the OUT direction (48 ± 13% increase, $P$ = 0.0047, $n$ = 6) and varied significantly with input velocity [$P$ = 0.0431 and 0.0194 for IN and OUT, respectively; analysis of variance (ANOVA) test], with the optimal velocity for direction sensitivity being similar to that of the somatic EPSP (2.0 ± 0.4 μm/μs) (Fig. 2, D and E). The spatial $Ca^{++}$ profiles along the dendrite were also different for the IN and OUT directions (Fig. 2, C and F).

What are the mechanisms underlying direction and velocity sensitivity in single dendrites? First, the somatic voltage responses to input sequences were markedly supralinear (Fig. 3A) (peak voltage = 223 ± 9% of the arithmetic sum, $P$ < 0.0001) and voltage-dependent (fig. S3, B to D) and did not exhibit a clear somatic threshold or a step increase in $dV/dt$ (where $V$ is voltage, and $t$ is time) (fig. S3A) (*13*, *15*), but rather developed gradually with increasing numbers of activated synapses (Fig. 3B). Next, we investigated the role of *N*-methyl-D-aspartate (NMDA) receptors (NMDARs), given their important contribution to dendritic nonlinearities in pyramidal cells (*13*, *16*–*18*, *24*). The NMDAR blocker D-AP5 abolished EPSP supralinearity (103 ± 3% of linear sum, $P$ = 0.336, $n$ = 8) (Fig.

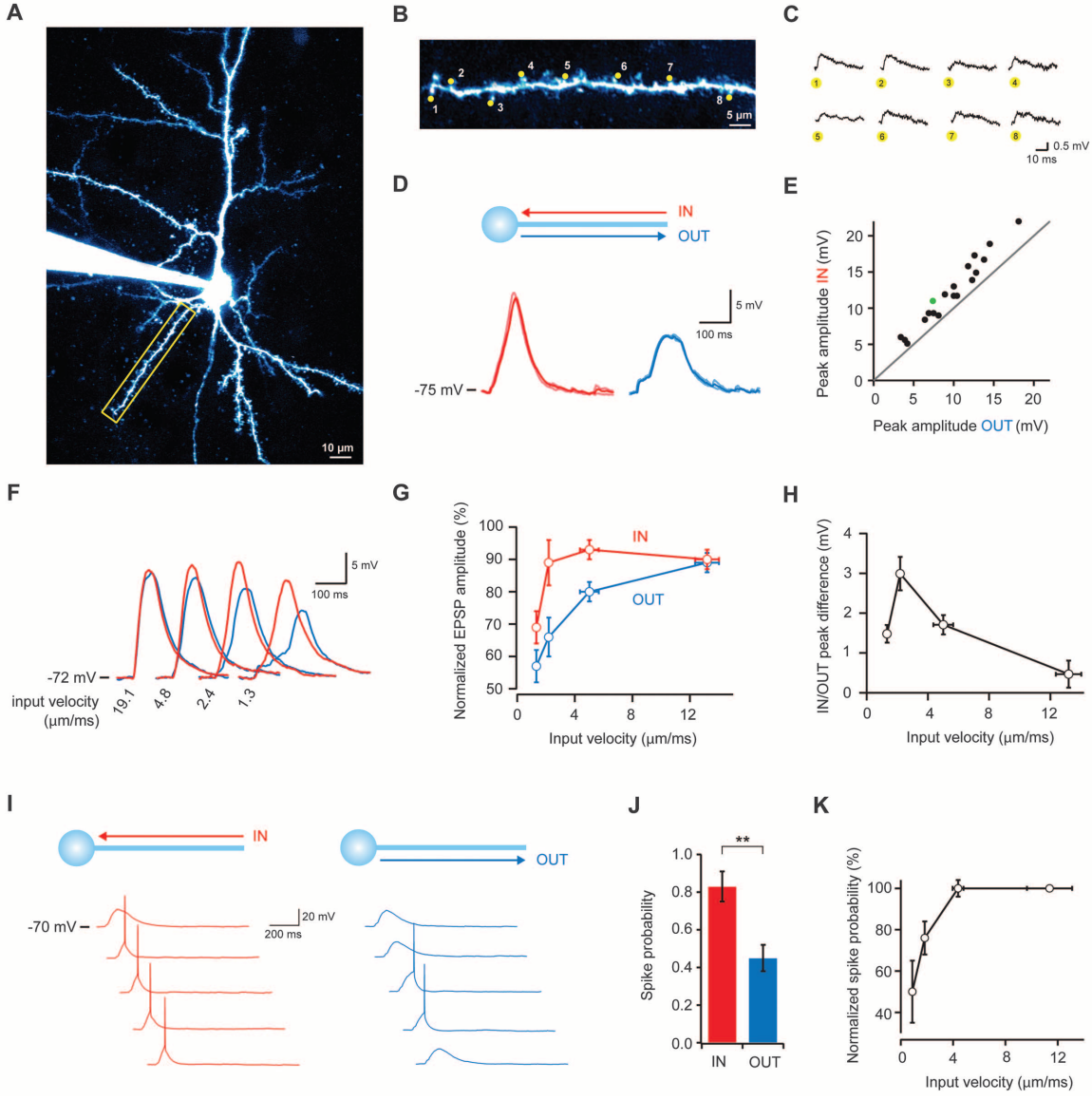


**Fig. 1.** Single dendrites are sensitive to the direction and velocity of synaptic input patterns. (**A**) Layer 2/3 pyramidal cell filled with Alexa 594 dye; yellow box indicates the selected dendrite. (**B**) Uncaging spots (yellow) along the selected dendrite. (**C**) Average individual uncaging responses at the soma. (**D**) Somatic responses to IN (red) and OUT (blue) directions at 2.3 μm/ms (averages denoted by bold lines). (**E**) Plot comparing peak amplitudes for IN and OUT sequences at the optimal velocity for direction selectivity [green circle, example shown in (D)]. (**F**) Direction-selective responses at different velocities. (**G**) Relation between peak voltage and input velocity (values normalized to the maximum response in the IN direction for each cell, $n$ = 15). Error bars indicate SEM. (**H**) Relation between direction selectivity and input velocity ($n$ = 15). (**I**) Direction selectivity of spike probability; population data shown in (**J**) (**$P$ = 0.0013, $n$ = 7). (**K**) Relation between spike probability and velocity ($n$ = 7, average of both directions).

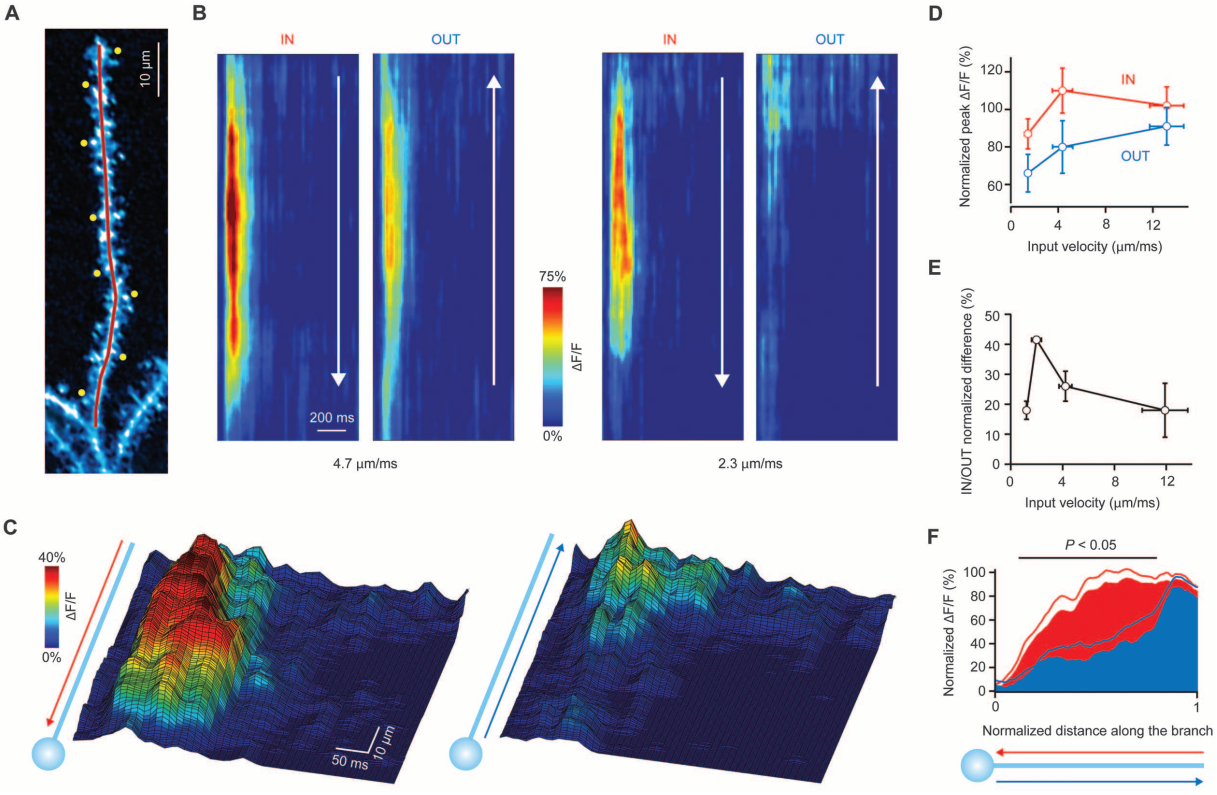


**Fig. 2.** Dendritic calcium influx is direction and velocity sensitive. (**A**) Basal dendrite of a layer 2/3 pyramidal neuron. Uncaging locations indicated in yellow; linescan profile used for $Ca^{++}$ imaging in red. (**B**) Spatiotemporal profile of $Ca^{++}$ signals triggered by IN and OUT input patterns at two different input velocities. (**C**) Three-dimensional plot of the data in (B) (2.3 μm/ms). (**D**) Relation between $Ca^{++}$ signals and input velocity ($\Delta F/F$ values, where $F$ is fluorescence, normalized to the mean $\Delta F/F$ of all velocities in the IN direction of each cell). Error bars indicate SEM. (**E**) Relation between direction selectivity of $Ca^{++}$ signals and input velocity. (**F**) Average spatial profile of the integrated $Ca^{++}$ transient across the dendrite ($n$ = 5 cells) (lines indicate SEM; bar indicates region of statistical significance).

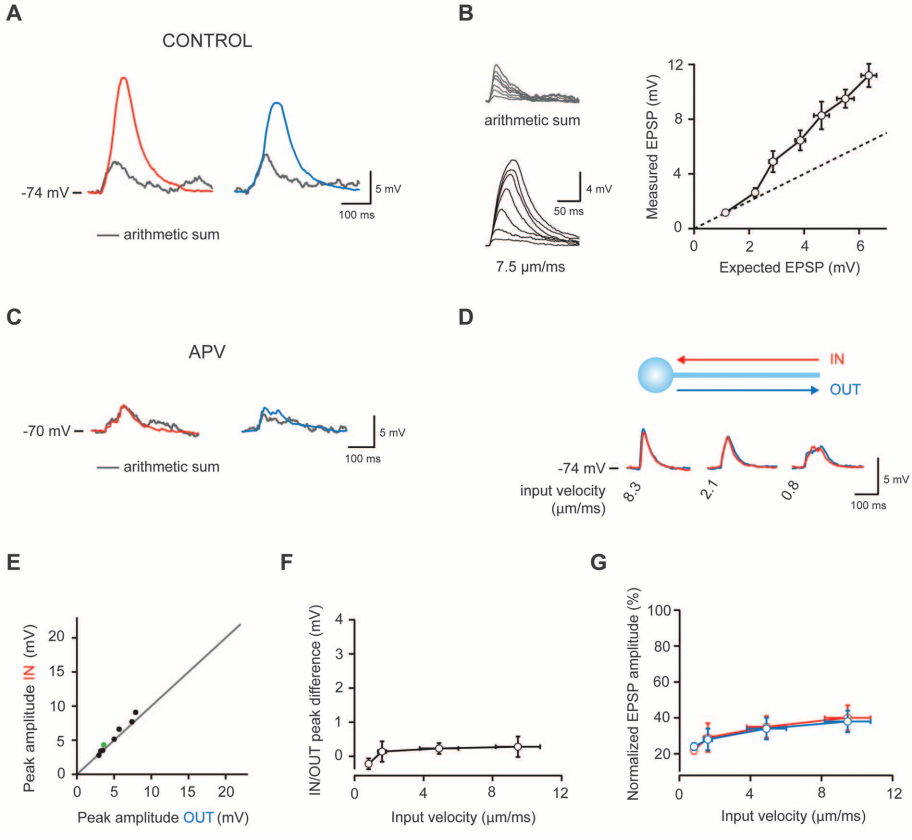


**Fig. 3.** NMDA receptor activation is required for robust velocity and direction coding. (**A**) Somatic responses to IN and OUT sequences (red and blue traces, respectively) and linear sum of the individual synaptic responses (gray traces). (**B**) (Left) Activating more synapses (1 to 7) produces EPSPs that are progressively larger than the linear sum of the individual responses. (Right) Summary plot of eight cells. Solid line, experimental data points; dashed line, unity line. Error bars indicate SEM. (**C**) Same as in (A), but in the presence of AP5, which blocks the supralinearity. (**D**) Velocity and direction sensitivity is abolished in AP5. (**E**) Comparing peak amplitudes for IN and OUT sequences at the optimal velocity for direction selectivity [green circle, example shown in (C)] (compare with Fig. 1E). (**F**) Summary plot of direction selectivity versus velocity (compare with Fig. 1G). (**G**) Reduced velocity sensitivity in AP5 (EPSPs normalized to the average IN maximum in control cells in the absence of D-(–)-2-amino-5-phosphonopentanoic acid) (compare with Fig. 1H).

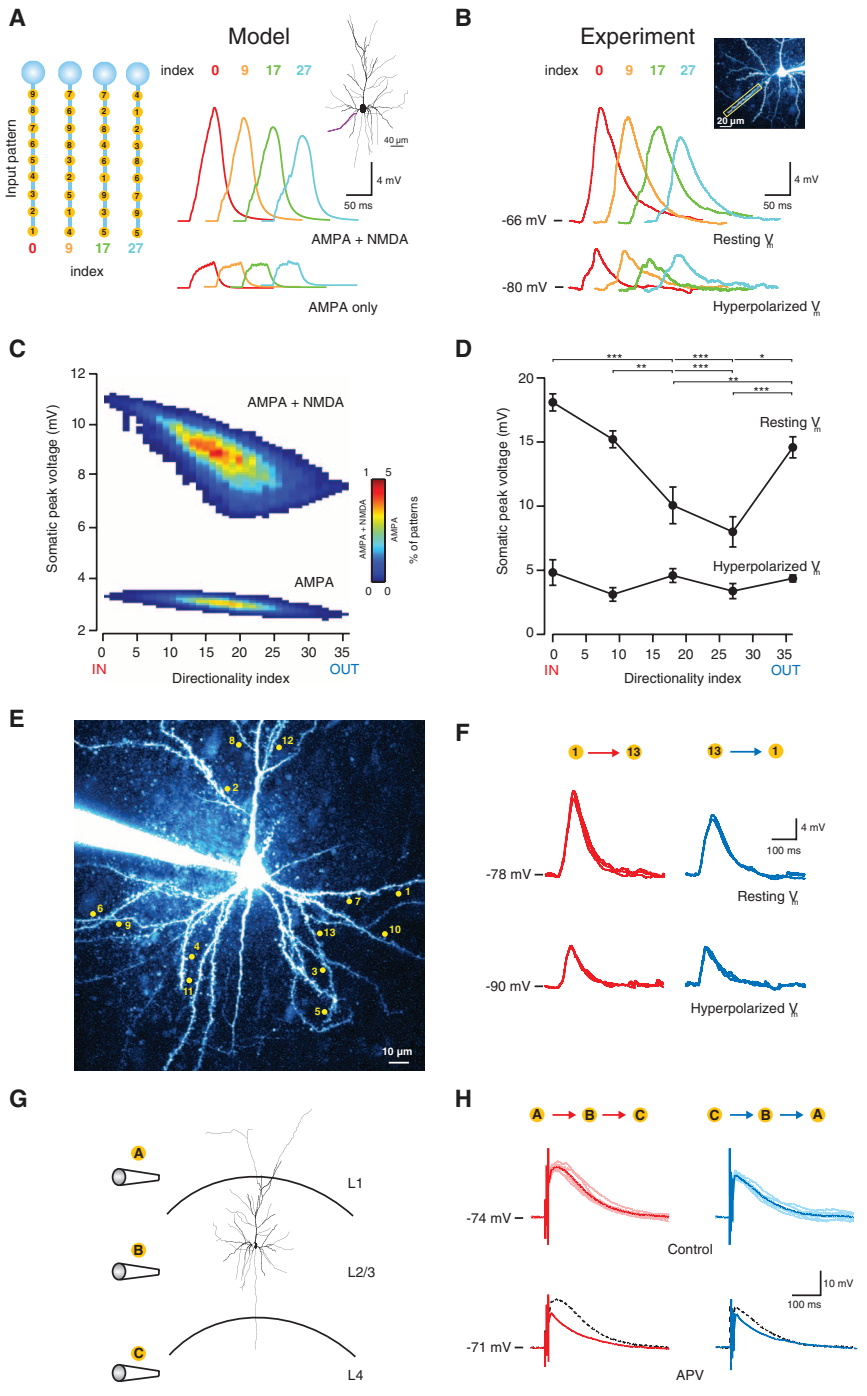


**Fig. 4.** Dendritic discrimination of complex input sequences. (**A**) Random patterns of nine inputs were generated and sorted by their directionality index (*35*). Four sample patterns (numbers showing activation order) and corresponding directionality index are shown. Patterns were played into a single dendrite in a pyramidal cell model or (**B**) experimentally in single pyramidal cell dendrites. The peak response is different for different patterns, and responses become similar with hyperpolarization (or without NMDA receptors in the model). (Inset) Dye-filled neuron with dendrite used in the experiment enclosed by a yellow box. Vm, membrane potential. (**C**) Pattern separability (measured by somatic peak EPSP distribution) was much greater with NMDA conductances present. (**D**) Peak EPSP voltage measured experimentally depends on input-pattern similarly to the model (C). Asterisks indicate significant differences between EPSP peaks for the example shown; hyperpolarization reduces the ability to discriminate different patterns. Error bars indicate SEM. (**E**) A layer 2/3 pyramidal cell with uncaging spots (yellow) randomly distributed across eight dendrites. (**F**) Somatic responses to sequential uncaging in forward (red traces) or reverse sequence (blue traces; averages denoted by bold lines) are different at resting potential and become similar upon hyperpolarization. (**G**) Three stimulation electrodes (denoted by letters A, B, and C) were placed in different cortical layers and activated in two different sequences. (**H**) The EPSP depends on the sequence and on NMDAR activation. Black dashed lines denote control response.

3C), consistent with amplification via NMDA-dependent regenerative signal boosting and NMDA spikes (*25*). The NMDAR blocker also abolished direction sensitivity (Fig. 3, D to F) (IN response 8 ± 3% larger than the OUT response; peak voltage difference of 0.4 ± 0.4 mV, significantly smaller than control, $P = 0.0011$) and velocity sensitivity (Fig. 3G), as well as any detectable dendritic calcium signals (fig. S4).

To probe the biophysical basis of direction sensitivity, we used a detailed compartmental model of layer 2/3 pyramidal cells. Direction sensitivity could be reproduced with a relatively simple model, with passive dendrites and synapses containing AMPA and NMDA conductances (fig. S5). The simulations showed that the mechanism of direction sensitivity in single dendrites results from the interaction of two factors: (i) the gradient of input impedance along the dendrite combined with (ii) the highly nonlinear voltage dependence of the NMDAR conductance. This leads to asymmetric recruitment of NMDA receptors when activating synapses in different sequences, such that sequences starting from regions of high input impedance (the tip of the dendrite) generate more initial local depolarization and, hence, more cumulative NMDAR activation. We verified the differential recruitment of nonlinearities between proximal and distal synapses with calcium imaging and glutamate uncaging in different regions of the same dendrite (fig. S6). The relative simplicity of this mechanism suggests that it should be general; indeed, the vast majority of dendrites across a wide range of morphologies exhibit sufficient impedance gradients to permit substantial direction sensitivity (fig. S7). We confirmed this experimentally by showing that neurons with very different morphologies—layer 5 pyramidal cells and hippocampal dentate gyrus granule cells—also exhibit robust direction sensitivity (fig. S8). This is especially relevant in the latter, as they receive layered input from the entorhinal cortex, with the lateral cortex projecting distally and the medial cortex proximally.

Can this mechanism be used to discriminate more complex patterns of input? We first assessed discrimination of random patterns by a single dendrite (Fig. 4, A and B). In both the model (Fig. 4, A and C) and the experiments (Fig. 4, B and D), different sequences of the same inputs produced a wide range of somatic EPSP amplitudes ($P < 0.05$, ANOVA on each cell; mean difference between experimentally tested patterns = 2.3 mV ± 0.22 mV; 39 ± 8% of all possible sequence comparisons were significant, $P < 0.05$, $t$ test with Bonferroni correction, $n = 7$), which was dependent on NMDA receptor activation (mean difference between patterns = 0.69 ± 0.13 mV, $P < 0.0001$) (Fig. 4, C and D). This is because synapses at different locations along the dendrite differentially influence each other, depending on their relative timing. The broad EPSP amplitude distribution reflects the discriminability of different sequences, with the likelihood of discriminating any two sequences (>1-mV

peak difference) being 40%. This distribution was insensitive to feedback inhibition but shifted to a smaller mean with the same variance with feedforward inhibition, suggesting that the same NMDA-dependent mechanism can represent the combined spatiotemporal sequence of excitation and inhibition (fig. S9). Whereas synaptic interactions are maximal if synapses are on the same dendrite, voltage can spread to other parts of the dendritic tree, the extent depending on the tree geometry and biophysical properties. We therefore examined whether neurons could also discriminate patterns of input delivered to multiple dendrites. By activating multiple spines across several dendrites, it was possible to discriminate the response to activation of different sequences of distributed input patterns (Fig. 4, E and F) (mean EPSP peak difference = 3.3 ± 0.8 mV, $P$ = 0.0065, $n$ = 9; tested sequences had no net directionality; see fig. S10, E and F, and supporting online material text). This discriminability was fully reproduced by our model (fig. S10, A and B) and was severely reduced upon hyperpolarization (0.58 ± 0.2 mV, $P$ = 0.0003) (Fig. 4F) and by block of NMDA receptors (fig. S10B). We further extended these results using the model, in which input sequences could be reliably discriminated over a wide range of spatial input distributions (fig. S10, C and D) and experimentally by showing that sequential activation of multiple input pathways could be discriminated (mean peak difference in control 2.8 ± 0.3 mV versus 0.9 ± 0.2 mV in AP5, $P$ = 0.0121, $n$ = 6) (Fig. 4, G and H).

We have shown that single cortical pyramidal cell dendrites can encode the temporal sequence of synaptic input. The underlying mechanism relies on the interplay between nonlinear activation of synaptic NMDA receptors and the impedance gradient along dendritic branches, two fundamental biophysical features common to most neurons in the brain. The active, regenerative nature of this mechanism contrasts with the classic, passive directional selectivity proposed by Rall (*19*), which requires electrotonically very long dendrites. Instead, the NMDA-dependent mechanism produced strong sensitivity to the direction of synaptic input, even in short pyramidal cell dendrites, making it more general and sensitive to synaptic input, robust against timing jitter, and further enhanced and tunable by depolarization [such as in network UP states (*26*, *27*)]. Different input sequences also lead to differential dendritic $Ca^{++}$ signals, raising the possibility that they will engage plasticity mechanisms to different extents (*28*, *29*). The large dynamic range conferred by NMDA receptor activation allowed for high discriminability of multiple temporal sequences, both when inputs were on the same dendrite or when they were dispersed over the dendritic tree. This further extends the range of computational and plasticity mechanisms that have recently been described in dendrites (*10*, *13*, *15–18*, *30*, *31*). In particular, this sensitivity to temporal input sequences may be relevant for detecting features of sensory stimuli and for encoding the speed and directionality of waves of activity propagating in the cortex (*32–34*). It is also especially relevant for circuits with layered input such as the hippocampus, where this mechanism could be used by dentate gyrus granule cells to directly detect the sequence of entorhinal cortex activation. These computations are conventionally thought to be implemented at the level of neural populations, and thus, our results represent a demonstration of the power of dendrites for solving computational problems in the brain.

### References and Notes


1. M. Meister, L. Lagnado, D. A. Baylor, *Science* **270**, 1207 (1995).
2. R. C. deCharms, M. M. Merzenich, *Nature* **381**, 610 (1996).
3. M. Wehr, G. Laurent, *Nature* **384**, 162 (1996).
4. R. S. Johansson, I. Birznieks, *Nat. Neurosci.* **7**, 170 (2004).
5. S. Thorpe, A. Delorme, R. Van Rullen, *Neural Networks* **14**, 715 (2001).
6. R. Gütig, H. Sompolinsky, *Nat. Neurosci.* **9**, 420 (2006).
7. A. Lazar, G. Pipa, J. Triesch, *Front. Comput. Neurosci.* **3**, 23 (2009).
8. J. C. Magee, *Nat. Rev. Neurosci.* **1**, 181 (2000).
9. D. Johnston, R. Narayanan, *Trends Neurosci.* **31**, 309 (2008).
10. M. London, M. Häusser, *Annu. Rev. Neurosci.* **28**, 503 (2005).
11. J. Schiller, Y. Schiller, G. Stuart, B. Sakmann, *J. Physiol.* **505**, 605 (1997).
12. N. L. Golding, N. Spruston, *Neuron* **21**, 1189 (1998).
13. J. Schiller, G. Major, H. J. Koester, Y. Schiller, *Nature* **404**, 285 (2000).
14. S. R. Williams, G. J. Stuart, *Trends Neurosci.* **26**, 147 (2003).
15. A. Losonczy, J. C. Magee, *Neuron* **50**, 291 (2006).
16. P. Poirazi, T. Brannon, B. W. Mel, *Neuron* **37**, 989 (2003).
17. B. W. Mel, *J. Neurophysiol.* **70**, 1086 (1993).
18. G. Major, A. Polsky, W. Denk, J. Schiller, D. W. Tank, *J. Neurophysiol.* **99**, 2584 (2008).
19. W. Rall, in *Neural Theory and Modeling*, R. Reiss, Ed. (Stanford Univ. Press, Stanford, CA, 1964), pp. 73–97.
20. T. Euler, P. B. Detwiler, W. Denk, *Nature* **418**, 845 (2002).
21. H. B. Barlow, W. R. Levick, *J. Physiol.* **178**, 477 (1965).
22. L. J. Borg-Graham, N. M. Grzywacz, in *Single Neuron Computation*, T. McKenna, J. Davis, Z. F. Zornetzer, Eds. (Academic Press, San Diego, CA, 1992), pp. 347–376.
23. M. Matsuzaki *et al.*, *Nat. Neurosci.* **4**, 1086 (2001).
24. M. E. Larkum, T. Nevian, M. Sandler, A. Polsky, J. Schiller, *Science* **325**, 756 (2009).
25. J. Schiller, Y. Schiller, *Curr. Opin. Neurobiol.* **11**, 343 (2001).
26. M. Steriade, A. Nuñez, F. Amzica, *J. Neurosci.* **13**, 3252 (1993).
27. M. V. Sanchez-Vives, D. A. McCormick, *Nat. Neurosci.* **3**, 1027 (2000).
28. N. L. Golding, N. P. Staff, N. Spruston, *Nature* **418**, 326 (2002).
29. P. J. Sjöström, E. A. Rancz, A. Roth, M. Häusser, *Physiol. Rev.* **88**, 769 (2008).
30. U. Gordon, A. Polsky, J. Schiller, *J. Neurosci.* **26**, 12717 (2006).
31. A. Losonczy, J. K. Makara, J. C. Magee, *Nature* **452**, 436 (2008).
32. F. Han, N. Caporale, Y. Dan, *Neuron* **60**, 321 (2008).
33. S. H. Lee, R. Blake, D. J. Heeger, *Nat. Neurosci.* **8**, 22 (2005).
34. I. Ferezou, S. Bolea, C. C. Petersen, *Neuron* **50**, 617 (2006).

35. Materials and methods are available as supporting material on *Science* Online.

36. We thank M. London, A. Roth, P. Dayan, J. Jack, and S. Smith for discussions; B. Judkewitz for help with image acquisition software; and C. Schmidt-Hieber for help with hippocampal granule cell experiments. This work was supported by grants from the Wellcome Trust and the Gatsby Charitable Foundation.


### Supporting Online Material

www.sciencemag.org/cgi/content/full/science.1189664/DC1
Materials and Methods
SOM Text
Figs. S1 to S18
References


16 March 2010; accepted 28 July 2010
Published online 12 August 2010;
10.1126/science.1189664
Include this information when citing this paper.

# Dendritic Discrimination of Temporal Input Sequences in Cortical Neurons

Tiago Branco, Beverley A. Clark, and Michael Husser

*Science*, **329** (5999), .
DOI: 10.1126/science.1189664

**Discriminating Dendrites**

Can dendrites read out spatiotemporal input sequences? Combining two-photon glutamate uncaging and two-photon calcium imaging, electrophysiology, and computational modeling, Branco *et al.* (p. 1671, published online 12 August; see the Perspective by Destexhe) discovered that single dendrites were indeed sensitive to both the direction and velocity of synaptic inputs. This direction- and velocity-sensitivity was measurable with only a few inputs and should thus be engaged frequently during normal brain function.







*Science* (ISSN 1095-9203) is published by the American Association for the Advancement of Science. 1200 New York Avenue NW, Washington, DC 20005. The title *Science* is a registered trademark of AAAS.